Contribution from the Department of Chemistry,
Texas A&M University, College Station, Texas 77843

Theoretical Studies of Inorganic and Organometallic Reaction Mechanisms. 5. Substitution Reactions of 17- and 18-Electron Transition-Metal Hexacarbonyl Complexes

Zhenyang Lin and Michael B. Hall*

Received January 17, 1992

Ab initio calculations with effective core potential have been used to study the mechanism of substitution reactions of 17-electron and 18-electron (e^-) transition-metal hexacarbonyl complexes. Pseudo-C_{2v} transition states were found for the substitution reactions investigated in this paper. The significant difference in the substitution reaction rates between 17-e^- and 18-e^- hexacarbonyl complexes is attributed to the significant difference in the valence-electron charge distributions of the corresponding transition states. The Laplacian of the valence-electron density indicates that the single-electron difference between the 19-e^- and 20-e^- transition states leads to a significant difference in the valence-electron charge concentrations. The angle between the two charge concentrations which face the entering and leaving ligands for a 20-e^- transition state is much smaller than that for a 19-e^- one. The more open coordination site of the 19-e^- system allows more effective bonding of the entering/leaving ligands to the central metal atom simultaneously. Therefore, the transition state is much more stable for the substitution reactions of 17-e^- transition-metal complexes.

Introduction

While most low-oxidation-state organometallic complexes conform to the closed-shell electronic configuration of the 18-electron rule, there has appeared an increasing number of reasonably stable 17-electron (e^-) metal-centered radicals.[1] Recent kinetic studies have shown that these electronically unsaturated species are exceptionally substitution labile.[2] For example, it has been shown that the first CO substitution of the vanadium hexacarbonyl, $V(CO)_6$, by phosphine ligands is about 10^{10} times faster than that of the analogous 18-e^- chromium complex, $Cr(CO)_6$.[3]

In the ligand substitution reactions, four types of reaction mechanisms are generally considered. They are D (dissociative), I_d (dissociative interchange), I_a (associative interchange), and A (associative). Although initial work on substitution of $M(CO)_6$ (M = Cr, Mo, and W) by amines indicated a simple D mechanism, later work has shown that a two-term rate law is applicable in reactions with amines, phosphines, and even acetonitrile.[1c] These kinetic studies showed competing D and I_d pathways. Thus, from the kinetic evidence, substitution reactions of 17-e^- metal carbonyl complexes proceed via a low-energy associative mechanism while those of 18-e^- complexes proceed via a dissociative or dissociative interchange one.[1-3]

The substitutional lability and associative mechanism of 17-e^- metal complexes have been explained qualitatively in terms of formation of a two-center, three-electron bond in the 19-e^- transition state or intermediate. More recently, Therien and Trogler employed SCF–X_α–DV molecular orbital calculations to discuss the possible modes of nucleophilic attacks on the metal carbonyl radicals constrained to ideal octahedral, trigonal-bipyramidal, square-pyramidal, and tetrahedral geometries.[4] However, the limitation of the SCF–X_α–DV method in estimating total energies prevented them from obtaining more quantitative results about the reaction's potential energy surface such as activation energies and geometries of transition states or intermediates. In this paper, ab initio quantum chemical calculations are used to study the associative mechanisms in the substitution reactions of the 17-e^- metal hexacarbonyls, $M(CO)_6$ (M = V, Nb, and Ta), to determine geometries of their transition states, and to test the level of theory required to predict the experimental observations. For comparison, we also made parallel calculations on an associative reaction path for the substitution reaction of the analogous 18-e^- complexes, $M(CO)_6$ (M = Cr, Mo and W). The effect of electron correlation on these systems will also be discussed in detail.

Theoretical Details

Ab initio effective core potentials were employed in the molecular orbital calculations. All geometries were optimized at the restricted Hartree–Fock (HF) level. The effect of electron correlation was studied by using single reference all-single-and-double-excitation (CISD) calculations at the HF optimized geometries.

In the effective core potentials (ECP), the outermost core orbitals which correspond to an ns^2np^6 configuration for the three transition series atoms were treated explicitly on an equal footing with the nd and $(n+1)$s valence orbitals. The basis sets of the first, second, and third transition series atoms were (541/41/41), (541/41/31), and (541/41/21), respectively.[5] For ligand atoms, the effective core potentials and double-ζ basis sets of Stevens, Basch, and Krauss were used.[6] [He] and [Ne] configurations were taken as cores for the first- and second-row main-group atoms. The basis for H consisted of a three Gaussian contraction from which the most diffuse component was split off to form a double-ζ basis.[7]

The CISD calculations used the HF results as starting solutions and the ground states as the single references. The active spaces of the CISD calculations include all occupied orbitals except the lone pairs on oxygens and the core electrons, and 42 lowest out of 91 virtual orbitals. For example, the active space for a CISD calculation on the $Cr(CO)_7$ system with an ECP method includes 31 occupied orbitals consisting of 7 Cr—C bonding orbitals, 21 C≡O bonds, 3 d electron pairs, and 42 lowest virtual (unoccupied) orbitals. The four outermost core electron pairs ($3s^23p^6$) of Cr and seven lone pairs on oxygens were excluded in the active space. The total number of configurations for $Cr(CO)_7$ (and $W(CO)_7$) with C_{2v} symmetry is 213 130 while for $V(CO)_7$ (and $Ta(CO)_7$) it is 514 453. The limitation of the available computing facility prevented us from using a larger active space.

The estimation of the basis set superposition error (BSSE)[8,9] was made at HF and CISD (with an active space of d valence electrons and all virtual molecular orbitals) levels for fragment $W(CO)_5$, which was derived from the calculated transition state $W(CO)_7$ of the carbonyl exchange reaction $W(CO)_6 + CO$ where the two entering/leaving ligands were weakly bonded to the central metal atom. We did calculations for the $W(CO)_5$ fragment with the presence of ghost centers occupying the positions of the two

(1) (a) Baird, M. C. *Chem. Rev.* **1988**, *88*, 1217; (b) Trogler, W. C. *Int. J. Chem. Kinet.* **1987**, *19*, 1025; (c) Howell, J. A. S.; Burkinshaw, P. M. *Chem. Rev.* **1983**, *83*, 557.
(2) (a) Basolo, F. *Inorg. Chim. Acta* **1985**, *100*, 3; (b) Basolo, F. *Polyhedron* **1990**, *9*, 1503; (c) Basolo, F. *Pure Appl. Chem.* **1988**, *60*, 1193; (d) Herrington, T. R.; Brown, T. L. *J. Am. Chem. Soc.* **1985**, *107*, 5700.
(3) (a) Shi, Q. Z.; Richmond, T. G.; Trogler, W. C.; Basolo, F. *J. Am. Chem. Soc.* **1982**, *102*, 4032; (b) Shi, Q. Z.; Richmond, T. G.; Trogler, W. C.; Basolo, F. *J. Am. Chem. Soc.* **1984**, *104*, 71.
(4) Therien, M. J.; Trogler, W. C. *J. Am. Chem. Soc.* **1988**, *110*, 4942.
(5) Hay, P. J.; Wadt, W. R. *J. Chem. Phys.* **1985**, *82*, 299.
(6) Stevens, W. J.; Basch, H.; Krauss, M. *J. Chem. Phys.* **1984**, *81*, 6026.
(7) Hehre, W. J.; Stewart, R. F.; Pople, J. A. *J. Chem. Phys.* **1969**, *51*, 2657.
(8) Boys, S. F.; Bernardi, F. *Mol. Phys.* **1970**, *19*, 553.
(9) Loushin, S. K.; Liu, S. Y.; Dykstra, C. E. *J. Chem. Phys.* **1986**, *84*, 2720.

0020-1669/92/1331-2791$03.00/0

Table I. Activation Energies and Selected Structural Parameters of Hartree–Fock Transition States for $M(CO)_6 + CO$

reaction system	activation energy (kcal/mol)	structural parameters		activation energy difference	first CO dissociation energy
		α (deg)	M···CO (Å)		
$Cr(CO)_6 + CO$	19.1	62.5	4.23	2.7	20.3
$V(CO)_6 + CO$	16.9	61.4	4.22		
$Mo(CO)_6 + CO$	27.3	60.0	4.23	6.5	28.4
$Nb(CO)_6 + CO$	20.8	59.5	3.38		
$W(CO)_6 + CO$	35.8	57.4	3.91	15.0	37.7
$Ta(CO)_6 + CO$	20.8	70.0	2.29		

entering/leaving ligands, $(CO)_2$. The basis functions of the ghost centers are exactly the same as those used for C and O atoms. We also did a calculation for the $W(CO)_5$ fragment without ghost centers. The energy difference between these two calculations is 0.6 kcal/mol at the HF level and 0.7 kcal/mol at the CISD level. The basis set superposition error is, therefore, less than 1.0 kcal/mol in the metal–ligand weakly-bound region of the potential energy surface.

All calculations were performed with the GAMESS package.[10] The electron density and its Laplacian were plotted with the use of the program MOPLOT.[11] All GAMESS calculations were made at the Cornell National Supercomputer Facility on an IBM 3090-600VF and at the Supercomputer Center of Texas A&M University on a Cray Y-MP2/116.

Results and Discussions

Carbonyl Exchange Reactions of Hexacarbonyl Metal Complexes. Basing our reasoning on the principle of microscopic reversibility, we have shown in a previous paper[12] that the associative transition state or intermediate of a substitution reaction for a system with identical entering and leaving ligands can be found by doing geometry optimization on structures with a mirror or C_2 symmetry restriction relating the entering and leaving ligands. To obtain an approximate reaction coordinate, we start from this transition state or intermediate and let the leaving ligand dissociate by lengthening (and fixing) the metal to leaving ligand bond length, while optimizing the remaining geometric parameters. We repeat this procedure until the metal to leaving ligand bond length is larger than 6.0 Å, which we take as a bond-breaking limit. Thus, we can generate a total energy vs reaction coordinate relationship from transition state (or intermediate) to products. The other half of the reaction coordinate from reactants to transition state (or intermediate) is simply related to the first half by the mirror symmetry of the potential energy surface. The activation energy can be easily estimated by comparing the total energies of reactants and the transition state. Whether the initial stationary point is a transition state or an intermediate can be determined from the energy vs reaction coordinate plot.

Beginning with an exchange reaction along the associative path, we determined the most favorable mode of nucleophilic attack on $M(CO)_6$ (M, groups 5 and 6 metal atoms) octahedral metal complexes. We considered nucleophilic attack on both an octahedral face and an edge of the octahedral complex. The possible transition states (or intermediates) corresponding to the face- and edge-attacking modes are shown in **1** and **2**, respectively, when an adjacent ligand is assumed to be a leaving ligand. When an opposite ligand is a leaving ligand, geometries **3** and **4** will be the possible transition states (or intermediates). Preliminary calculations indicated that electron correlation was important for the first and second transition series metal 19-e$^-$ and 20-e$^-$ systems, but is much less important for those of third-row systems, particularly for Ta systems. Therefore, we optimized $Ta(CO)_7$ with geometries **1**–**4**. In the geometry optimizations, the 19th valence electron always occupies the lowest L–M–E antibonding orbital. The results showed that **1** had the lowest energy, while **2** and **4** were 6.0 and 10.9 kcal/mol higher than **1**, respectively, and **3** was not a local minimum. We also did an optimization for one other 7-coordinate geometry, **5**, with the restriction of M–L = M–E (see **5**). It is 3.0 kcal/mol higher than **1**. Together, all these results suggest that the face-attacking mode, which was also suggested from the result of SCF–X_α–DV calculations,[4] with an adjacent leaving ligand is most favorable.

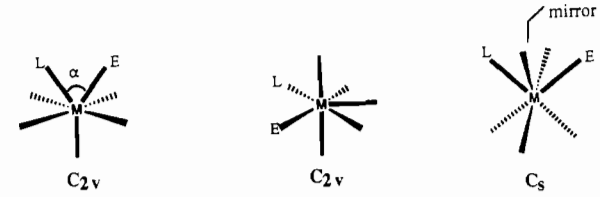

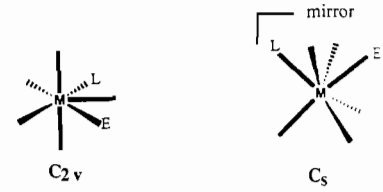

Following the procedure described above, we found the transition states (or intermediates) (**1**) and the activation energies for the associative exchange reactions of $M(CO)_6 + CO$ (M = Cr, V, Mo, Nb, W, and Ta) within the HF level. The activation energies and some selected structural parameters of the transition states are listed in Table I. We found no evidence of any intermediates nor significantly bent M–CO bonds in the transition states. The dissociation energies of the first carbonyl for 18-e$^-$ complexes were also calculated and are given in Table I. These dissociation energies were calculated by assuming the following process: $M(CO)_6 \rightarrow (CO)_5M\cdots CO$ (M···CO = 6.0 Å is taken as the bond-breaking limit), optimizing the structures of both $M(CO)_6$ and $(CO)_5M\cdots CO$ (Cr···CO = 6.0 Å), and then differencing their total energies.

Results (see Table I) showed that for the 18-e$^-$ complexes the calculated activation energy from the associative reaction mechanism and the calculated dissociation energy of the first CO were similar. This result is not too surprising when we consider that both entering and leaving ligands are far away from the metal center in the calculated transition state for the associative reaction (see Table I). Thus, this associative reaction, in fact, resembles an I_d mechanism. Since for each 18-e$^-$ complex the assumed associative mechanism is more than 1.0 kcal/mol lower in activation energy than the corresponding dissociative process, a value slightly greater than the basis set superposition error, the parallel comparison of associative reactions between 18-e$^-$ and 17-e$^-$ complexes is reasonably justified.

The 10^{10} multiplicative difference in the substitution reaction rates of $Cr(CO)_6$ and $V(CO)_6$ by phosphine observed in kinetic studies corresponds to a difference of 12–13 kcal/mol in the activation energy if we assume an Arrhenius expression for the rate constant, and similar preexponential factors. We can see from

(10) Guest, M. F. Daresbury Laboratory, Warrington WA4 4AD, U.K.
(11) Interactive MOPLOT: a package for the interactive display and analysis of molecular wavefunctions incorporating the programs MOPLOT (D. Lichtenburger), PLOTDEN (R. F. W. Bader, D. J. Kenworthy, P. M. Beddal, G. R. Runtz, and S. G. Anderson), SCHUSS (R. F. W. Bader, G. R. Runtz, S. G. Anderson, and F. W. Biegler-Koenig), and EXTREM (R. F. W. Bader and F. W. Biegler-Koenig); P. Sherwood and P. J. MacDougall, 1989.
(12) Lin, Z.; Hall, M. B. *Inorg. Chem.* **1991**, *30*, 646.

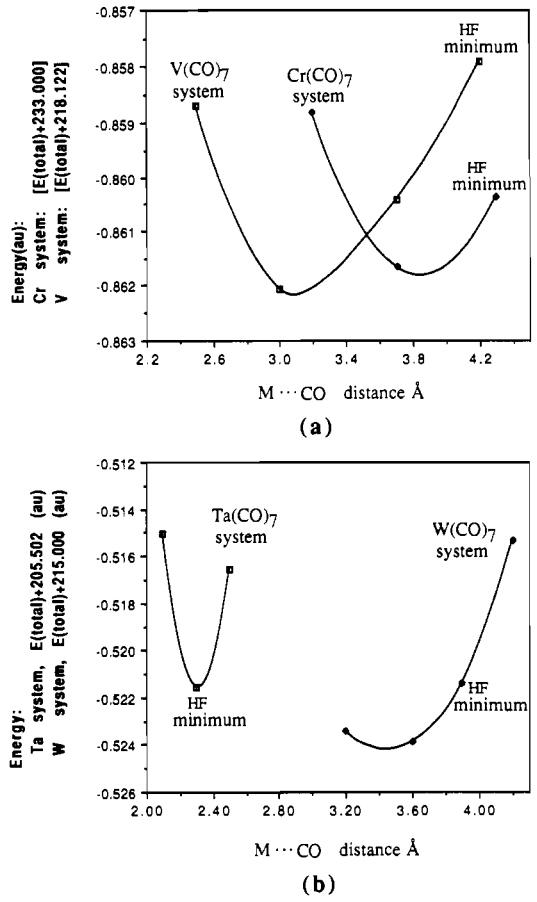

Figure 1. Total energies of CISD calculations vs the two equal M···CO distances for (a) $Cr(CO)_7$ and $V(CO)_7$ systems and (b) $W(CO)_7$ and $Ta(CO)_7$ systems. The geometry of the HF minima point in each curve corresponds to the optimized (ECP2-HF) C_{2v} structure (**1**). The geometries of the remaining points are obtained by optimizing the C_{2v} structures with fixed M···CO distances at the ECP2-HF level. The CISD calculations used the HF-SCF wave functions as starting solutions.

Table I that at the Hartree–Fock level only the third-row transition-metal systems give a significant difference (15.0 kcal/mol) between the substitution reactions of 17-e⁻ and 18-e⁻ metal complexes.

Together, all these results suggest that the electron correlation is responsible for underestimating the activation-energy difference of the 19-e⁻ and 20-e⁻ systems for the first and second transition series metals. To test this hypothesis, we performed CISD calculations on the transition states, $M(CO)_7$, for the reactions $Cr(CO)_6$ + CO, $V(CO)_6$ + CO, $W(CO)_6$ + CO, and $Ta(CO)_6$ + CO. We start with the HF optimized C_{2v} geometry (**1**), and then let the two entering/leaving ligands approach (or leave) the metal center by fixing the two equal M···CO distances and optimizing the remaining structural parameters within the HF level. Finally, we made CISD calculations on these partially optimized structures. The total energies of the CI calculations vs M···CO distances are plotted in Figure 1. It can be seen from the figure that the CI minimum for the V system deviates substantially from the HF minimum. The CI minima for both Cr and W systems also deviate from their HF minima, but the deviation is less than that for the V system. However, the CI minimum for the Ta system is consistent with the HF minimum. At first glance, the potential energy curve for the Ta system (see Figure 1b) seems too narrow. However, the frequency for the symmetrical vibration mode was calculated to be small (ca. 216 cm^{-1}) on the basis of the curvature of the curve in Figure 1b. We also used the same procedure to test the effect of electron correlation on the Ta···CO bond angles. Results showed no CI dependence of Ta···CO angles. Although the activation energy difference between the Cr and V reactions at CI level increases to 4.9 kcal/mol, it is still much smaller than the experimental value. The CI calculations give a higher activation energy difference of 22.0 kcal/mol between reactions of $W(CO)_6$ + CO and $Ta(CO)_6$ + CO. Thus, even for third-row transition metals, the HF calculations underestimate the difference in the activation energies.

At this stage, we could continue our search for a large enough basis set and CI expansion to reproduce the significant activation-energy difference between Cr and V systems. Alternatively, we can employ other model systems, which are chemically and physically similar to Cr and V systems, to explore the origin for their significant difference. To reduce the computational expenses, we have chosen the second approach for this study and left the former approach for a future study.

In summary, the HF calculations on the Ta transition-metal carbonyl system provides geometries consistent with CI calculations. Although the W system shows slightly CI dependence, the geometries obtained from both the HF and CI energy minima are similar. All the calculations above are based on the CO exchange reactions, but for most transition-metal carbonyls, the rates of the CO exchange reactions are slow.[2b] As a more realistic system, we shall use $Ta(CO)_6$ + PH_3 and $W(CO)_6$ + PH_3 as model reactions. Hence, the stronger nucleophile may modify the results discussed above.

Carbonyl Substitution Reactions of $M(CO)_6$ by Phosphine. When the entering and leaving ligands are not identical, the procedure described above cannot be used to determine the transition state (or intermediate) and reaction coordinates of substitution reactions. For a general substitution reaction, $L_nMX + Y \rightarrow L_nMXY \rightarrow L_nMY + X$, the reaction path must connect reactants (L_nMX + Y) at A to the products (L_nMX + Y) at B in the two-dimensional potential surface shown as follows:

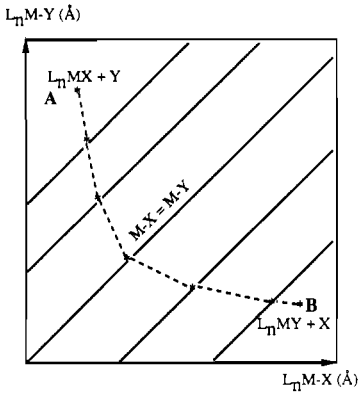

The diagonal lines, which can be expressed as the equation M–Y = M–X + R (or R = M–Y – M–X), where M–Y is the metal to entering ligand distance and M–X is the metal to leaving ligand distance, must cross the true reaction path. The crossing points along the line R = M–Y – M–X are the energy minima along this line. Therefore, we can obtain a reaction path by optimizing a system L_nMXY with a geometrical restriction of constant R, where R = M–Y – M–X. In theory, $R = \infty$ corresponds to reactants and $R = -\infty$ to products; in practice, we assume $|R|$ = 4.0 Å to be close enough to the bond-breaking limit. Thus, we optimize the L_nMXY system at fixed R values from R = 4.0 Å to R = –4.0 Å to obtain the total energy vs the reaction coordinate (R).

Following this procedure, we obtain the total energy vs R for the reaction of $Ta(CO)_6$ + PH_3 shown in Figure 2a. The corresponding optimized geometries are shown in Chart I. In the geometry optimization, the internal coordinates of PH_3 were fixed by using standard bond lengths and bond angles,[13] and a C_s symmetry was imposed (see Chart I). An activation energy of 21.7 kcal/mol is calculated. When the same procedure is used for the $W(CO)_6$ + PH_3 reaction, we obtain the total energy vs reaction coordinate shown in Figure 2b and the corresponding geometries shown in Chart II. The activation energy for this

(13) Hehre, W. J.; Ditchfield, R.; Steward, R. F.; Pople, J. A. *J. Chem. Phys.* **1970**, *52*, 2769.

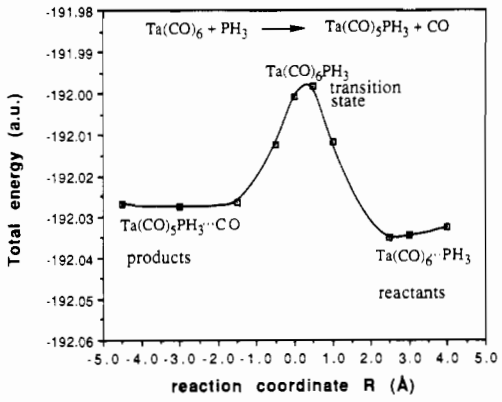

(a)

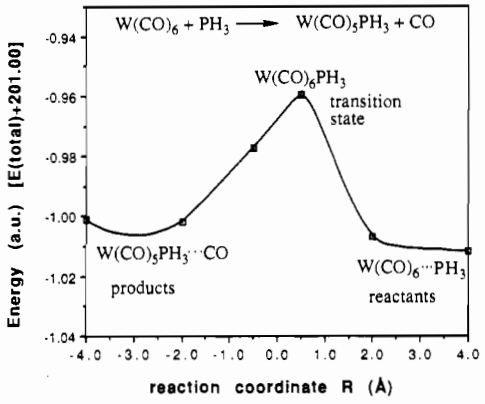

(b)

Figure 2. Potential energy curve along the reaction coordinate for reactions of $Ta(CO)_6 + PH_3$ (a) and $W(CO)_6 + PH_3$ (b) (ECP2-HF result).

reaction is 32.8 kcal/mol. Again, a significant difference in activation energies (ca. 11 kcal/mol) is observed for the two (18-e⁻ and 17-e⁻) substitution reactions. Although CI calculations will give a higher activation energy difference (vide supra), they will not alter our conclusion for third-row systems and were not performed.

Examining the energy curves (Figure 2) and the related geometries in both reaction paths (Charts I and II), we take Chart I, structure D, and Chart II, structure C, as approximate transition states of $Ta(CO)_6 + PH_3$ and $W(CO)_6 + PH_3$ reactions, respectively. Both transition states are similar to the C_{2v} symmetry of the transition states for the exchange reactions discussed above and have small entering ligand to metal to leaving ligand angles. The bending of the leaving CO ligand observed in the post-transition state will be discussed in more detail later.

Orbital and Density Analysis. Since all of the transition states we found in the exchange and substitution reactions have a C_{2v} or C_{2v}-like geometry (**1**), a simple picture of the molecular orbital interaction in a C_{2v} ML_7 (**1**) transition-metal molecule is helpful in illustrating these systems. Figure 3 shows the interaction diagram between a square-pyramidal ML_5 fragment and the two entering/leaving ligand σ orbitals in the yz plane. As we can see, the d_{yz} orbital of the "t_{2g}" set is antibonding and the $d_{x^2-y^2}$ orbital is slightly antibonding. Since in our models the structural changes from reactants to products are entirely restricted to the yz plane, the electron density contributed by the d_{yz} and $d_{x^2-y^2}$ orbitals is of primary importance in the reaction process. For a 20-e⁻ ML_7 system, the d_{yz} orbital is doubly occupied while for a 19-e⁻ ML_7 system it is singly occupied.

Before providing a more detailed discussion, we plot the Laplacian of the total electron density, i.e., $-\nabla^2\rho$,[14,15] from ab initio

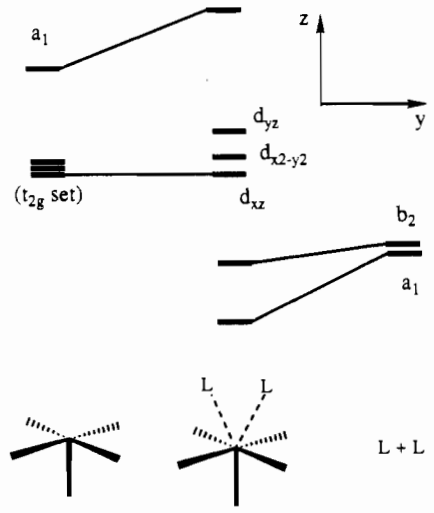

Figure 3. Molecular orbital interaction scheme for a C_{2v} ML_7 (**1**) transition-metal molecule.

Scheme I

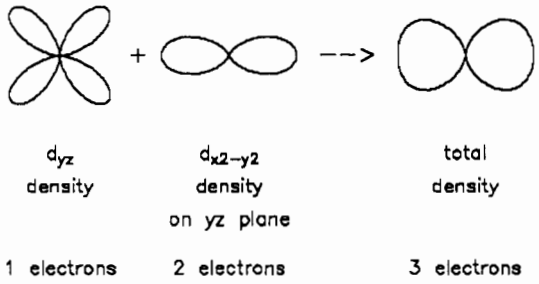

Scheme II

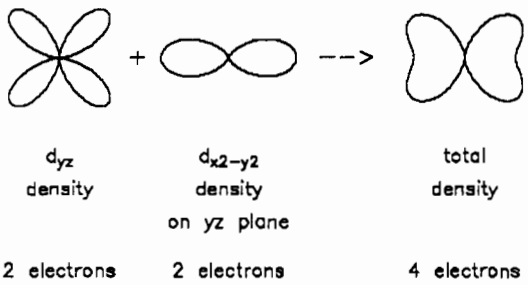

calculations (HF/ECP) on the transition states of carbonyl exchange reactions. Figure 4 shows $-\nabla^2\rho$ plots on the reaction plane (yz plane) of the transition states (**1**) for $Ta(CO)_7$ (Figure 4a) and $W(CO)_7$ (Figure 4b) systems, respectively. In the contour displays, solid lines denote $-\nabla^2\rho > 0$, where the electron charge is locally concentrated, and dashed lines denote $-\nabla^2\rho < 0$, where the electron charge is locally depleted. On the left side of Figure 4, the Laplacian of the electron density from all the electrons in the ECP (HF) calculations is plotted while on the right side the Laplacian of the valence-electron density, which was obtained by subtracting the outermost core-electron ($5s^25p^6$) contributions, is plotted. As we can see from the left side of Figure 4, the difference between $Ta(CO)_7$ and $W(CO)_7$ systems is not very clear in the $-\nabla^2\rho$ plots from the ECP total electron density. However, the difference in the valence-electron $-\nabla^2\rho$ plots is clearly seen from the right side of the figure. In the 19-e⁻ $Ta(CO)_7$ system, the valence electrons have two charge concentrations in the yz plane, while in the 20-e⁻ $W(CO)_7$ system, four charge concentrations are seen.

A qualitative argument based on an orbital model is helpful for understanding these observations. Simple schemes are given here to illustrate the valence-electron density on the yz plane, when the d_{yz} orbital is singly occupied (Scheme I) and doubly occupied

(14) Bader, R. F. W.; MacDougall, P. J.; Lau, C. D. H. *J. Am. Chem. Soc.* **1984**, *106*, 1594.

(15) Bader, R. F. W. *Acc. Chem. Res.* **1985**, *18*, 9.

Chart I

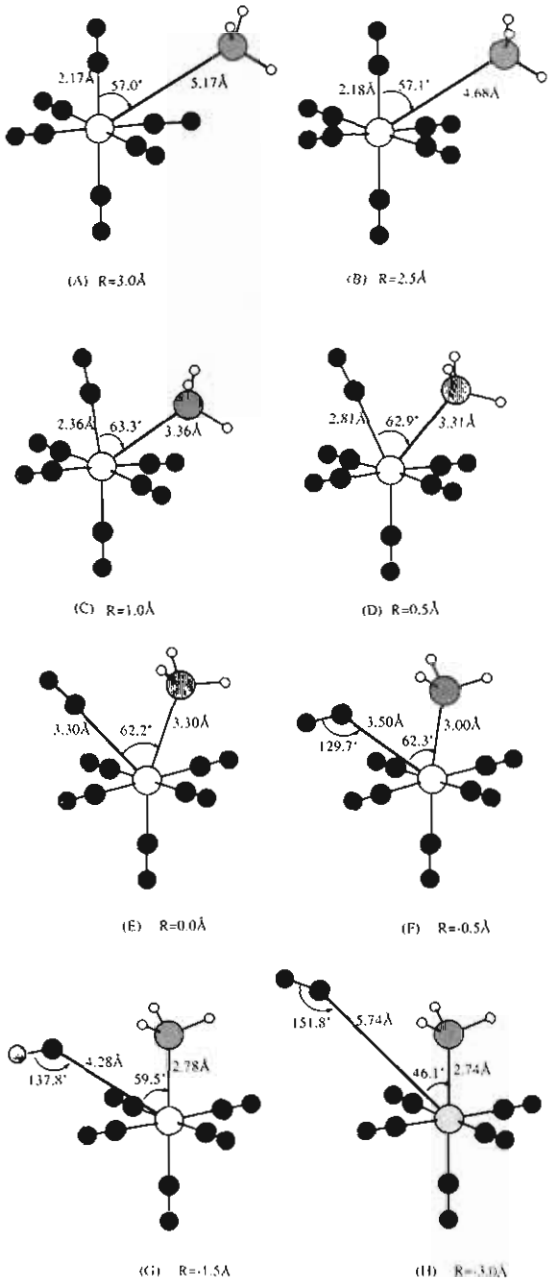

(Scheme II). The plots in the illustrations are made by considering only the angular dependence of the wave functions since the radial dependence is similar for each d orbital. These schemes are consistent with actual calculations of electron density maps of atomic Ta. Since Scheme I corresponds a 19-e$^-$ system and Scheme II to a 20-e$^-$ system, we can see that the single-electron difference leads to a significant difference in the electron density. For the 19-e$^-$ system, the valence-electron density in the reaction plane gives two maxima in the $+y$ and $-y$ directions. The valence-electron density for a 20-e$^-$ system gives four maxima. For the 20-e$^-$ system, the angle between the two maxima in the $+z$ direction (toward the entering/leaving ligands) is 109.46°, which is calculated from the angular spherical harmonics. The small angle prevents both the entering and leaving ligands from bonding effectively to the central metal atom since the width of the hole (electron charge depletion; see also Figure 4)[16] toward the entering/leaving ligands is much smaller than that for the 19-e$^-$ system. Therefore, the associative transition state for a substitution reaction of an 18-e$^-$ transition-metal complex is expected to be energetically much higher than that of its analogous 17-e$^-$ complex.

(16) Macdougall, P. J.; Bader, R. F. W. *Can. J. Chem.* **1986**, *64*, 1496.

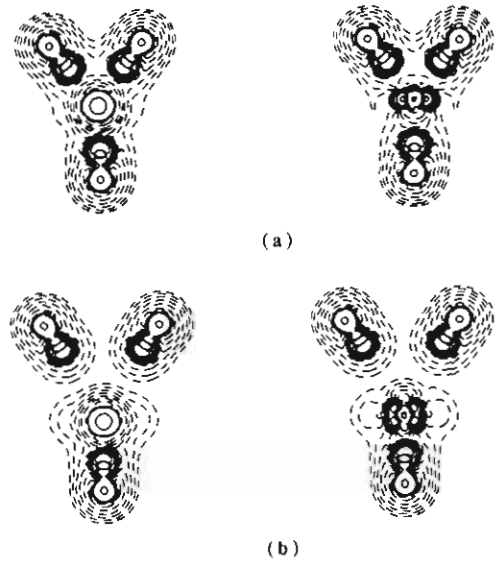

Figure 4. $-\nabla^2\rho$ on the reaction plane of the transition states in the $Ta(CO)_6$ + CO (a) and $W(CO)_6$ + CO (b) carbonyl exchange reactions: left side, based on the total electron density directly from ECP2 results; right side, based on the valence-electron-only density.

Chart II

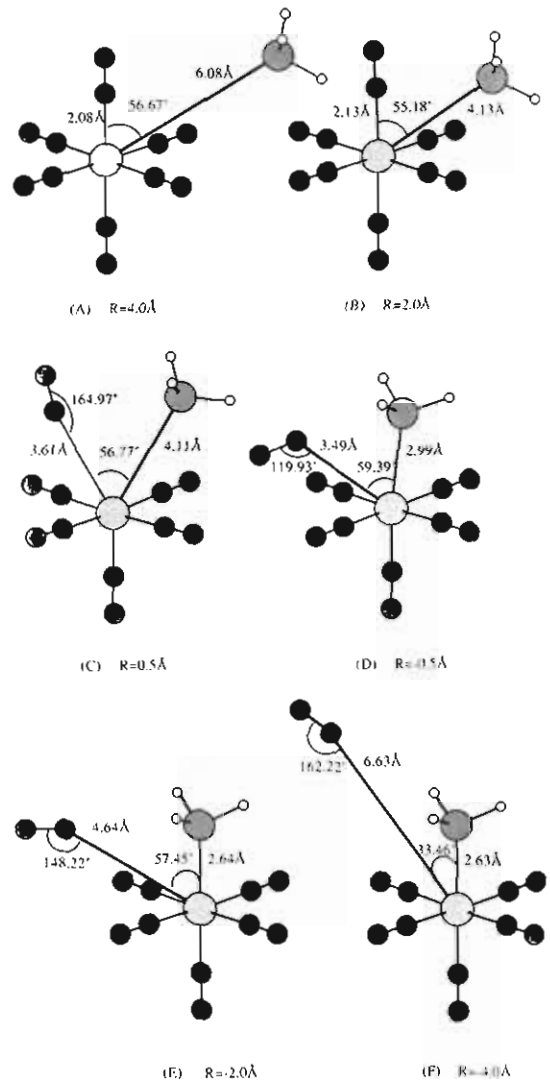

This qualitative orbital argument is strongly supported by the ab initio results (see Figure 4, the $-\nabla^2\rho$ plots).

The valence-electron $-\nabla^2\rho$ plots based on the geometries of Charts I and II for $Ta(CO)_6 + PH_3$ and $W(CO)_6 + PH_3$ reactions

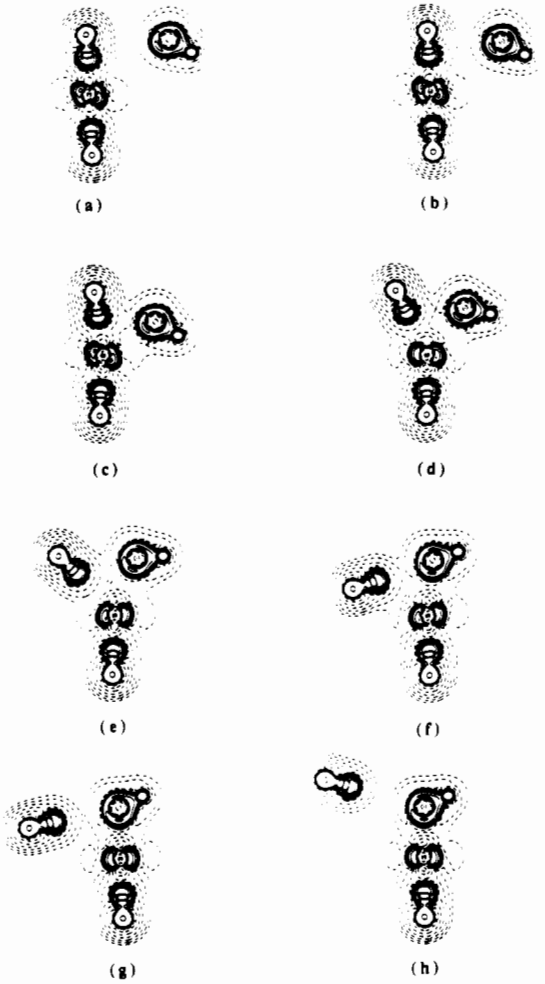

Figure 5. $-\nabla^2\rho$ (valence-electron-only) along the reaction coordinate on the reaction plane for the reaction of $Ta(CO)_6 + PH_3$.

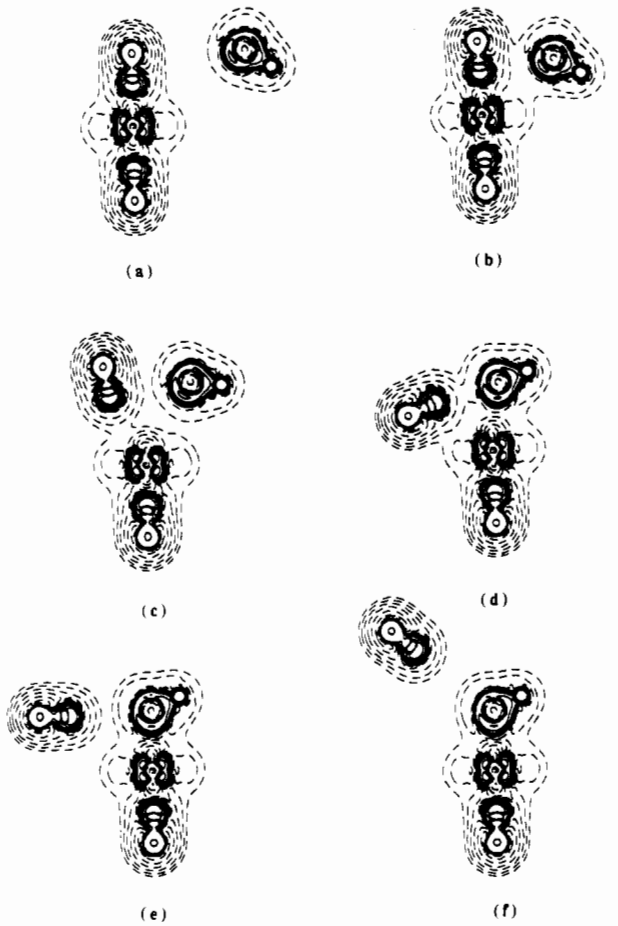

Figure 6. $-\nabla^2\rho$ (valence-electron-only) along the reaction coordinate on the reaction plane for the reaction of $W(CO)_6 + PH_3$.

are also shown in Figures 5 and 6. In these figures, the detailed changes of valence-electron charge distributions along the reaction paths, which correspond to Charts I and II, are illustrated. The $-\nabla^2\rho$ plots of the assumed transition states (Chart I, structure D, and Chart II, structure C) correspond to Figures 5d and 6c. Again, Figure 5d shows two charge concentrations while Figure 6c shows four. The asymmetric behavior of the two charge concentrations in Figure 5 will be discussed later.

In summary, the significant difference in the substitution reaction rates of 18-e$^-$ and 17-e$^-$ transition-metal carbonyl complexes is reflected in the significant difference in the valence-electron distributions of their associative transition states. In the substitution reaction of the 18-e$^-$ metal carbonyl complex, the associative transition state corresponds to a 20-e$^-$ system. The valence-electron charge concentrations are located directly in the directions of metal–entering/leaving ligand bonds in the transition state. For a 19-e$^-$ system, the two maxima in the charge concentration are not directed toward the entering/leaving ligands. The structures of transition states (Chart I, structure D, and Chart II, structure C) clearly show that much shorter metal–entering/leaving ligand bonds in the 19-e$^-$ system than in the 20-e$^-$ system are observed. Therefore, a relatively more stable transition state is observed for the substitution reaction of a 17-e$^-$ transition-metal complex.

Checking the detailed changes in the electron charge distributions along the reaction paths for the two systems (Figures 5 and 6), we also see that the distortion of the charge concentrations in the central atom for the 19-e$^-$ system is much greater than that for the 20-e$^-$ system. Little distortion is observed for the latter. These observations are possible due to the less contracted d orbitals for group 5 atoms which form 17-e$^-$ metal complexes. The diffuse nature of d orbitals for group 5 atoms leads an easier rehybridization. The nature of the entering ligand is also possibly responsible for these observations because of the strong σ donating ability of phosphine and its tendency to form a strong σ bond to the metal center. Therefore, the distortion in the charge concentrations is not observed in those structures close to the products in the reaction of $Ta(CO)_6 + PH_3$ (see Figure 5) since the CO is a much weaker σ donor.

The discussion above may be responsible for the unexpected substitution inertness of some 17-e$^-$ transition-metal complexes. For example, it was reported recently that the $[LM(CO)_3]^+$ (L = 1,4,7-tribenzyl-1,4,7-triazacyclononane; M = Cr, Mo, W) 17-e$^-$ radicals do not display the substitution lability.[17] In these radicals, the metal centers are group 6 atoms. In addition, each radical possesses a positive charge in the complex. The d orbitals in the metal centers must be very contracted, and therefore the rehybridization ability is very weak. It has been reported that the rate of the CO exchange reaction of $V(CO)_6$ is very slow with a half-life of 7 h.[2b] This is due, at least in part, to the poor σ donating ability of the CO ligand.

In both Charts I and II, no significant bending M–CO (CO is the leaving ligand) is observed from the reactants to the transition states. However, as the reactions proceed from the transition states to products, the leaving CO ligand bends. This phenomenon can be explained through the σ and π interactions between the central metal atom and the leaving carbonyl. Before the CO dissociates, the σ and π interactions are very strong and bending is disfavored. When the CO starts to dissociate, the σ interaction becomes repulsive. Therefore, the bending strengthens the π interaction and reduces σ antibonding. The slight bend W–CO in the assumed transition state of the 20-e$^-$ system (Chart II, structure C) is the result of beginning CO dissociation (W–CO

(17) Beissel, T.; Vedova, B. S. P. C. D.; Wieghardt, K.; Boese, R. *Inorg. Chem.* **1990**, *29*, 1736.

3.61 Å). Thus, the I_d transition state for the 20-e⁻ system has more bond breaking than the associative transition state for the 19-e⁻ system.

Conclusion

The ab initio results on the substitution reactions of 17-e⁻ and 18-e⁻ octahedral hexacarbonyl transition-metal complexes indicates a pseudo-C_{2v} transition state. No intermediate in the reactions is observed. For the substitution reaction of a 17-e⁻ metal complex, the simple two-center three-electron bond picture is not so obvious in our calculations. It is better to view both entering and leaving ligands on equal footing. From Figure 3, the occupation of one electron in the d_{yz} orbital in the 19-e⁻ system suggests a three-center five-electron bond in the transition state for a substitution reaction of a 17-e⁻ transition-metal complex.

The most important factor in the experimental observation of a significant difference in the substitution reaction rates of 18-e⁻ and 17-e⁻ metal complexes is the significant difference in the valence-electron charge distributions of the corresponding transition states. The analysis of the Laplacian of the valence electron density in the calculated transition states indicates that the single electron difference between 19-e⁻ and 20-e⁻ systems leads to a significant difference in the valence-electron charge concentrations. The angle between the two charge concentrations toward the entering and leaving ligands for the 20-e⁻ system is much smaller than that for the 19-e⁻ system. More open coordination sites for the 19-e⁻ system allow an effective bonding of the central metal atom to the entering/leaving ligands simultaneously in the transition state. Therefore, the transition state is much more stable for the substitution reactions of 17-e⁻ transition-metal complexes.

Acknowledgment. We thank the National Science Foundation (Grant No. CHE 91-13634) and the Robert A. Welch Foundation (Grant No. A-648) for financial support and M. F. Guest for providing the GAMESS package of programs. This research was conducted in part with use of the Cornell National Supercomputer Facility, a resource for the Center for Theory and Simulation in Science and Engineering at Cornell University, which is funded in part by the National Science Foundation, New York, and the IBM Corp.

Contribution from the Department of Inorganic Chemistry, Indian Association for the Cultivation of Science, Calcutta 700 032, India

On Pearson's HSAB Principle

Dipankar Datta

Received August 6, 1991

Some 35 examples of the exchange reaction AB + CD = AC + BD (type 1), for which Pearson's HSAB (hard–soft acid–base) principle was originally devised, are examined in terms of the experimental or calculated hardness (η) values of the various species involved. The calculation of the η values has been done at the MNDO level by using $\eta = (\epsilon_{LUMO} - \epsilon_{HOMO})/2$, where ϵ is energy, LUMO indicates the lowest unoccupied molecular orbital, and HOMO is the highest occupied molecular orbital. In the case of some 75 molecules it is found that the η values calculated at the MNDO level match quite well with the experimental η values. The examples of the exchange reaction are so chosen that the experimental hardnesses of at least three of the four species involved in a particular example are known. From the present study it is concluded that an exchange reaction proceeds in a direction so as to produce the hardest possible species and the average value of the hardnesses of the products is greater than that of the reactants in a reaction of type 1. The results are explained in terms of the chemical reactivity of the four molecules involved in a particular example. Of the 35 examples studied there are only 5 exceptions.

Introduction

In 1963 Pearson[1] introduced the hard–soft acid–base (HSAB) principle which states that "hard acids prefer to coordinate to hard bases and soft acids to soft bases".[2] This apparently simple statement has been used successfully by Pearson to rationalize a variety of chemical information.[3] But the concept of hardness or softness (inverse of hardness) remained qualitative till 1983. The qualitative definition of hardness uses the idea of polarizability; a less polarizable species is hard and a more easily polarized one, soft. For ions of similar charge the ratio of charge and radius can be used for assessing their relative polarizability. However no numbers could be assigned to a particular species before 1983. The quantitative definition[4] given by eq 1 relates hardness η of

$$\eta = (IP - EA)/2 \quad (1)$$

any chemical species to its ionization potential IP and electron affinity EA. Incidentally, the average of IP and EA gives the electronegativity (χ) of a neutral species (eq 2). By applying

$$\chi = (IP + EA)/2 \quad (2)$$

Koopmans' theorem, Pearson has shown[5] that for closed-shell species 2η is equal to the gap between the HOMO (highest occupied molecular orbital) and LUMO (lowest unoccupied molecular orbital (eq 3). In eq 3, ϵ represents energy. Since in a

$$\eta = (\epsilon_{LUMO} - \epsilon_{HOMO})/2 \quad (3)$$

chemical reaction, as first shown by Fukui,[6] of all the molecular orbitals of the reactants the HOMO and LUMO participate most actively, η is expected to be a index of chemical reactivity. This has been felt by a number of workers.[7,8] In any case, that the thermodynamic stability of a chemical species increases with the increase in the HOMO–LUMO gap is now well recognized.[9-13] Though hardness has been quantified to the extent possible, a complete theoretical proof for the statement of the HSAB principle is still not available. Very recently Parr and co-workers have provided only a partial proof.[14] Earlier Nalewajski[15] tried to justify the essence of the statement qualitatively using a modified form of the definition of electronegativity given by Iczkowski and

(1) Pearson, R. G. *J. Am. Chem. Soc.* **1963**, *85*, 3533.
(2) Pearson, R. G. *J. Chem. Educ.* **1987**, *64*, 561.
(3) Pearson, R. G. *Coord. Chem. Rev.* **1990**, *100*, 403 and references therein.
(4) Parr, R. G.; Pearson, R. G. *J. Am. Chem. Soc.* **1983**, *105*, 7512.
(5) Pearson, R. G. *Proc. Natl. Acad. Sci. U.S.A.* **1986**, *89*, 1827.
(6) Fukui, K.; Yonezawa, T.; Shingu, H. *J. Chem. Phys.* **1952**, *20*, 722.
(7) Datta, D.; Sharma, G. T. *Inorg. Chem.* **1987**, *26*, 329.
(8) Zhou, Z.; Parr, R. G. *J. Am. Chem. Soc.* **1990**, *112*, 5720 and references therein.
(9) Pearson, R. G. *J. Org. Chem.* **1989**, *54*, 1423.
(10) Burdett, J. K.; Coddens, B. A. *Inorg. Chem.* **1988**, *27*, 3259.
(11) Faust, W. L. *Science* **1989**, *245*, 37.
(12) Zhou, Z.; Parr, R. G.; Garst, J. F. *Tetrahedron Lett.* **1988**, 4843.
(13) Zhou, Z.; Parr, R. G. *J. Am. Chem. Soc.* **1989**, *111*, 7371.
(14) Chattaraj, P. K.; Lee, H.; Parr, R. G. *J. Am. Chem. Soc.* **1991**, *113*, 1855.
(15) Nalewajski, R. F. *J. Am. Chem. Soc.* **1984**, *106*, 944.

0020-1669/92/1331-2797$03.00/0